Static Disorder in Excitation Energies of the Fenna-Matthews-Olson Protein: Structure-Based Theory Meets Experiment

Marten Chaillet, Florian Lengauer, Julian Adolphs, Frank Müh, Alexander Fokas, Daniel Cole, Alex W. Chin, Thomas Renger

Static Disorder in Excitation Energies of the Fenna-Matthews-Olson Protein: Structure-Based Theory Meets Experiment

Marten L. Chaillet,[†] Florian Lengauer,[‡] Julian Adolphs,[¶] Frank Müh,[‡] Alexander S. Fokas,[§] Daniel J. Cole,[‖] Alex W. Chin,[⊥] and Thomas Renger[*,‡]

†*Bijvoet Centre for Biomolecular Research, University of Utrecht, Heidelberglaan 8, 3584 CS Utrecht, The Netherlands*

‡*Institute of Theoretical Physics, Johannes Kepler University Linz, Altenberger Str. 69, 4040 Linz, Austria*

¶*Leibniz Institute for Agricultural Engineering and Bioeconomy, Max-Eyth-Allee 100, 14469 Potsdam, Germany*

§*TCM Group, Cavendish Laboratory, 19 J J Thomson Avenue, Cambridge CB3 0HE, United Kingdom*

‖*School of Natural and Environmental Sciences, Newcastle University, Newcastle upon Tyne NE1 7RU, United Kingdom*

⊥*Centre National de la Recherce Scientifique, Institute des Nanosciences de Paris, Sorbonne Universite, Paris, France*

E-mail: thomas.renger@jku.at

Abstract

Inhomogeneous broadening of optical lines of the Fenna-Matthews-Olson (FMO) light harvesting protein is investigated by combining a Monte-Carlo sampling of low-energy conformational substates of the protein with a quantum chemical/electrostatic calculation of local transition energies (site energies) of the pigments. The good agreement between the optical spectra calculated for the inhomogeneous ensemble and the experimental data demonstrates that electrostatics is the dominant contributor to static disorder in site energies. Rotamers of polar amino acid side chains are found to cause bimodal distribution functions of site energy shifts, that can be probed by hole-burning and single molecule spectroscopy. When summing over the large number of contributions, the resulting distribution functions of the site energies become Gaussians, and the correlations in site energy fluctuations at different sites practically average to zero. These results demonstrate that static disorder in the FMO protein is in the realm of the central limit theorem of statistics.

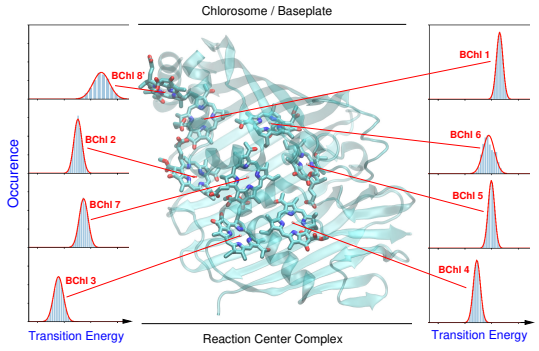

The conformational motion of proteins spans many orders of magnitude in time, ranging from femtosecond vibrations of individual atoms and molecular groups via the nanosecond regime of concerted motion of structural elements like groups of residues towards the microsecond and longer time scales of large scale conformational transitions of whole protein domains. This multi-scale flexibility allows the protein to perform such complex functions as light-driven catalysis. In photosynthesis, sun light is absorbed by light-harvesting antennae, and

transferred to a reaction center, where the light-energy is converted into free energy of chemical compounds. The Fenna-Matthews-Olson (FMO) protein is a trimeric pigment-protein complex (PPC) (Fig. S1) that connects an outer antenna system (chlorosome) with the reaction center complex in green sulfur bacteria. Every monomer binds 8 BChl *a* pigments (Fig. 1). 2D electronic spectroscopy was developed and applied to resolve details of the energy transfer in the FMO protein[1,2] and in whole cells[3] of green sulfur bacteria. Small amplitude long-lived coherent oscillations found in these 2D spectra[4–8] gave birth to the field of quantum biology.[9,10]

A full appreciation of the spectroscopic data requires structure-based simulations, which are, however, difficult because of the complexity of this system. Multi-scale methods[11,12] are needed in order to obtain a realistic picture of the light-harvesting dynamics. The workhorse in such a description has been a Frenkel exciton Hamiltonian $H = H_{\rm ex} + H_{\rm ex-vib} + H_{\rm vib}$ expanded in the basis of localized excited states $|m\rangle$ of the PPC. In the latter state, pigment m is excited and all other pigments are in their electronic ground state. The exciton part of this Hamiltonian reads

$$H_{\rm ex}(c) = \sum_m E_m(c)|m\rangle\langle m| + \sum_{m,n}^{m\neq n} V_{mn}(c)|m\rangle\langle n|\,, \tag{1}$$

where $E_m(c)$ and $V_{mn}(c)$ are the local transition energy, termed site energy, of pigment m and the excitonic coupling between pigments m and n, respectively. Both quantities depend on the conformation c of the PPC, which changes slowly compared to the excited state lifetime (fs to ns) of the pigments. Any fast conformational motion that modulates the excitonic couplings and transition energies is contained in the exciton-vibrational coupling Hamiltonian $H_{\rm ex-vib}$ and the nuclear motion is described by $H_{\rm vib}$ (explicit expressions for these Hamiltonians are given in the supporting information (SI)).

In linear spectroscopy, in good approximation, the eigenstates $|M\rangle = \sum_m c_m^{(M)}|m\rangle$ of $H_{\rm ex}$ are excited, where the eigenenergies E_M correspond to the transition energies seen

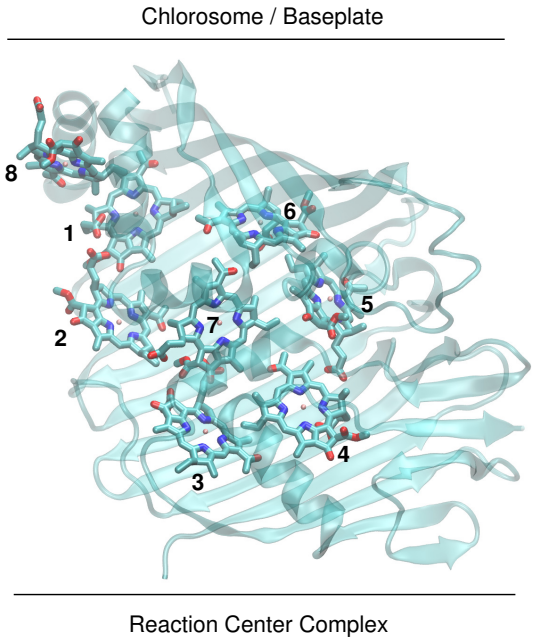

Figure 1: Monomeric subunit of the trimeric FMO protein from *P. aestuarii*, which connects the outer antenna system (chlorosomes) with the reaction center complex in an orientation as indicated in this figure. The protein part is shown in transparent ribbon style and the pigments are numbered as in PDB file 3EOJ.[13] The phytyl tails of the pigments were truncated for better visibility. The complete structure of the FMO trimer is shown in Fig. S1. Graphics prepared with VMD.[14]

in the spectra. The coefficients $c_m^{(M)}$ of the eigenstates are obtained from the respective eigenvectors of the exciton matrix $H_{\rm ex}$. These coefficients together with the local transition dipole moments $\mathbf{d}_m$ determine the amplitudes of the optical lines seen in the absorption spectrum, which is obtained as

$$\alpha(\omega) \propto \omega \left\langle \sum_M |d_M|^2 D_M(\omega) \right\rangle_c , \tag{2}$$

where the transition dipole moment $\mathbf{d}_M$ of exciton state $|M\rangle$ reads $\mathbf{d}_M = \sum_m c_m^{(M)} \mathbf{d}_m$. The lineshape function $D_M(\omega)$, obtained by taking into account the exciton-vibrational coupling, contains homogeneous line broadening caused by the excitation of vibrational sidebands and exciton relaxation (more details, including also circular and linear dichroism spectra, are given below and in the SI). The inhomogeneous lineshape, finally, is obtained by performing

an average over static disorder in site energies and excitonic couplings, denoted as $\langle ... \rangle_c$.

The determination of (mean) site energies E_m and excitonic couplings V_{mn} of the FMO protein has been a problem for many decades.[15] Major progress concerning the site energies was obtained by Aartsma and coworkers,[16] who recognized that using a smaller effective dipole strength of the pigments in the calculation of excitonic couplings allows one to find site energies that fit linear absorption, linear dichroism and circular dichroism spectra. The low effective dipole strength was explained by quantum chemical/electrostatic calculations.[17] It was recognized that there is a gradient in local transition energies towards BChls 3 and 4, which are located on one side of the FMO protein. Based on energy transfer calculations, it was concluded that efficient light-harvesting requires BChls 3 and 4 to be the linker pigments between the FMO protein and the reaction center complex.[17] This prediction was confirmed experimentally by Blankenship and coworkers using chemical labeling of solvent-exposed groups and mass spectrometry.[18]

Attempts of a structure-based explanation of the site energy values were reported using various multi-scale approaches.[19–26] Some of these methods aim at a fully ab-initio description, without using any adjustable parameters.[22–26] In other simplified approaches, the intermolecular electrostatic pigment-protein coupling is evaluated,[11,19–21] and the obtained site energies are adjusted typically within a ± 60 cm^{-1} window from a fit of the optical spectra. It was recognized that the energy sink at BChl 3 is caused by the electric field of the backbone of two α-helices and by a hydrogen bonding network involving a hydrogen bond between a tyrosine and the keto group of BChl 3.[19] In recent years, the latter prediction has been verified in a site-directed mutation study, where this Tyr was replaced by Phe.[27]

The fluctuations of site energies of the BChl pigments of the FMO protein have been characterized theoretically by quantum mechanic / molecular mechanics (QM/MM) approaches.[24,28–33] The main focus has been on the fast fluctuations that are described by the spectral density of the exciton-vibrational coupling. The latter is related to the autocorrelation function of the site energy fluctuations, which has been calculated by combining

classical molecular dynamics (MD) simulations of the complex with QC calculations of optical transition energies of the pigments.[28,30] In such combinations, one has to be careful about the fact that the potential energy surfaces of the pigments are different in a classical and in a quantum description. Different strategies exist to avoid this geometry mismatch problem,[24,29,31–38] which artificially enhances the intrapigment contributions to the variation of site energies. One can either find a suitable interpolation between the MM and the QM potential energy surfaces of the pigments,[24,32,33,36] calculate the intermolecular and the intrapigment contributions to the site energy modulations separately,[29,31,34] taking special care for the intrapigment part, or neglect the latter.[39–41] The intermolecular contribution to the variation in site energies was calculated by combining the electrostatic charge density coupling (CDC) method,[20] that will be explained in more detail below, with classical MD[29,31,34] or normal mode[39] calculations. Alternatively, it was obtained in QM/MM simulations by subtracting from the full site energy variations the intrapigment contributions, obtained by switching off the environment in the calculation of site energies.[34,40,41] The intrapigment contribution to the site energy variation was obtained by using a quantum mechanic normal mode analysis (NMA) either on the isolated geometry optimized pigment[34] or on a QM optimized potential energy surface of the pigment along the classical MD trajectories.[29,31] Alternatively, the geometry mismatch problem has been tackled by quantum chemical calculations of the intrapigment potential energy surfaces using semi-empirical,[35], tight-binding density functional theory (DFT)[38] or DFT[37] methods and treating only the protein environment by classical force fields. However, such approaches are numerically very costly.

The focus of the present work lies on site energy variations that are much slower than excited state lifetimes (fs to ns) and give rise to static disorder causing an inhomogeneous broadening of optical lines. The underlying slow diffusive conformational motion of the protein is anharmonic and, therefore, cannot be captured with a NMA. MD simulations in principle are able to describe such conformational transitions, however, long simulation times are required and very likely local free energy barriers prevent a complete sampling

of phase space. Nevertheless, by time-averaging site energies in QM/MM calculations, first results on static site energy distribution functions were obtained.[33,40,41] The most detailed investigation of static disorder was reported by Rhee and coworkers,[33] who performed 100 ns QM/MM simulations of a monomeric subunit of the FMO protein using their interpolation scheme that avoids the geometry mismatch problem described above. By varying the window size for time-averaging of the site energy fluctuations, they were able to visualize different fluctuation regimes. In the regime of slow fluctuations (window size of 1 ns), they inferred a standard deviation of the time-windowed averages in the 20-50 cm^{-1} range corresponding to a full width at half maximum (FWHM) of 50-120 cm^{-1}, which is in the right range when compared with estimates of inhomogeneous distribution functions of site energies from the fit of optical spectra.[16,17,19,21,42]

An alternative and numerically efficient way to sample low-energy conformations of proteins is given by Monte-Carlo simulations, such as the framework rigidity optimized dynamic algorithm (FRODA).[43] This technique has been applied by some of us to the monomeric subunit of the FMO protein and to whole FMO trimers.[44,45] FRODA was combined with the TrEsp method[46] to investigate static disorder in excitonic couplings[44] and with linear scaling density functional theory (DFT) to study the correlation in site energy fluctuations between the two low-energy pigments BChl 3 and 4.[45] Due to the numerical costs of the linear scaling DFT calculations, that included also part of the environment (all atoms within a 15 Å cutoff radius of the pigment of interest), it was only possible to investigate a few different conformers of the FMO protein, generated from the first principal component of the MC trajectories. For these 9 conformations, an interesting correlation in site energies was found.[45] By restricting the DFT calculations to the first principal component, only the large scale motion of the protein was captured and the geometry mismatch problem, described above, could be avoided, since the pigment conformations were affected less enough. Correlations in dynamic site energy fluctuations have been investigated with MD simulations[47] and a normal mode analysis (NMA).[39] Whereas the MD simulations did not find any correlations,

in the NMA they appeared at very low vibrational frequencies.

In the present work, we combine the FRODA Monte Carlo technique for the sampling of low-energy conformational substates of the FMO protein with the efficient and robust electrostatic CDC method[20] for the calculation of site energy shifts. Since only intermolecular Coulomb couplings are calculated and the intrapigment contributions to the static site energy shifts are neglected, the geometry mismatch problem is avoided. In this way, it is possible to study a large number of different conformations, re-investigate the presence of correlations in static disorder, and provide a fully structure-based simulation of the inhomogeneous spectroscopic properties of the FMO protein.

The present simulations of static disorder in site energies and excitonic couplings are based on conformational substates of the FMO protein that were obtained in earlier work using a combination of the FIRST (Floppy Inclusions and Rigid Substructure Topography) and the FRODA (Framework Rigidity Optimized Dynamic Algorithm) algorithms.[43] Based on the geometry-optimized holo form of the crystal structure of FMO trimers of *Prosthecochloris aestuarii*,[13] FIRST was used to identify flexible and rigid regions of the complex taking into account covalent as well as non-covalent interactions. The "hard" degrees of freedom, containing the variation of covalent bond lengths and angles, as well as certain dihedral angles (e.g. for rotation around peptide bonds) define rigid clusters. The flexibility of the macromolecule is determined by rotation around single bonds connecting the rigid clusters. Hydrogen bonds and hydrophobic contacts were also considered in the definition of these clusters. A hydrogen bond energy cutoff value E_{cut} of -4.6 kcal/mol was applied and all hydrogen bonds with a larger binding energy were kept fixed during the subsequent Monte-Carlo generation of conformational substates with FRODA. 713 hydrogen bonds were identified in this way. In addition, 236 hydrophobic constraints were taken into account by not allowing atoms of two hydrophobic groups in van der Waals contact to separate by more than the sum of their van der Waals radii plus 0.5 Å in the course of the conformational sampling. Once the rigid cluster have been defined with FIRST using the graph-theoretical

pebble game algorithm,[48] FRODA is used for an efficient Monte Carlo sampling of the remaining flexibility of the macromolecule. In a Monte Carlo step, every atom is displaced in a random direction by a magnitude of 0.1 Å and ghost templates, containing the internal structure of the rigid clusters, are moved such as to minimize the distances between the new atom positions and the corresponding points on the ghost templates. In an iterative procedure atom positions and ghost templates are moved further until the atom positions fulfill the original constraints, that is, all atoms are close to the corresponding positions on the ghost templates. In comparison to the original structure the rigid clusters have moved without internal distortion, just by geometric means without using any potential energy function. Hence, FRODA is not rectricted to harmonic motion around some minimum of the potential energy surface. Repeating this procedure, a whole ensemble of conformational substates is obtained. The applied constraints allow for an efficient sampling of conformational states (scaling linearly with the number of atoms[43]) and restrict the conformations to that of the lowest energies connected by diffusive protein motion. The energy differences between the states are assumed to be so small that all states have the same statistical weight, independent on temperature. The downside of this simple approach lies in the neglect of long-range electrostatic and solvation effects which would alter the statistical weigths of the states and could shift the borders between flexible and rigid regions. Despite and because of these simplifications, FIRST/FRODA has proven to provide realistic conformational ensembles of proteins, as judged by comparison of atomic mobilities with experimental NMR data.[43] In the present work we provide further evidence by monitoring static disorder in local transiton energies of protein-bound pigments and ~~comparison~~ with experimental optical spectra of the inhomogeneous ensemble. A more detailed description of the FIRST/FRODA method and its application to the FMO protein can be found in earlier work.[43,44,48]

Using the FIRST/FRODA method, described above, 5200 conformations of the trimeric FMO protein were generated.[44] Local transition energies (site energies) of the 24 BChl *a* pigments are calculated with the charge density coupling (CDC) method for each of these

conformations.[20] The site energy of pigment m is obtained as

$$E_m(c) = E_0 + \sum_k \Delta E_m^{(k)}(c)\,, \tag{3}$$

where $\Delta E_m^{(k)}$ is the contribution by building block k of the PPC. It contains the difference in charge density coupling of the electronic ground state of this building block with the excited and the ground state of pigment m, reading

$$\Delta E_m^{(k)}(c) = \frac{1}{\epsilon_{\text{eff}}} \sum_{I,J} \frac{\left(q_I^{(m)}(1,1) - q_I^{(m)}(0,0)\right) q_J^{(k)}(0,0)}{|\mathbf{R}_I^{(m)}(c) - \mathbf{R}_J^{(k)}(c)|}\,. \tag{4}$$

Since the charge densities of the ground and excited state of pigment m and that of the ground state of the environment are approximated by atomic partial charges $q_I^{(m)}(0,0)$, $q_I^{(m)}(1,1)$ and $q_J^{(k)}(0,0)$, respectively, it is very simple to take into account a variation of the respective atomic positions $\mathbf{R}_I^{(m)}(c)$ and $\mathbf{R}_J^{(k)}(c)$ with respect to different conformations c of the complex. The two parameters E_0 and ϵ_{eff} are inferred from the center and the overall width, respectively, of the experimental optical spectra. In this way, uncertainties in the quantum chemical method and additional terms in the pigment-protein coupling (e.g. dispersive interactions) are implicitly taken into account. For the present system, we find optimal values of $E_0 = 12560$ cm^{-1} and $\epsilon_{\text{eff}} = 3.6$. The latter gives the best correlation between the mean site energies calculated with FRODA/CDC and the reference values from the literature (Fig. S2). The ground state partial charges of the protein were taken from the CHARMM22 force field,[49] assuming a standard protonation pattern of the titratable residues. The atomic partial charges of the pigments were obtained in earlier work[46] from a fit of the ab-initio electrostatic potential of the ground and excited state of geometry-optimized BChl *a*, computed with time-dependent DFT and the B3LYP exchange-correlation functional. The numerical values of the atomic partial charges of BChl *a* are given in Table S2. The statistical analysis of the site energies was done with octave.[50] Please note that the present approach takes

advantage of the stiffness of the closed-ring structure of the BChl *a* pigments, assuming that the intrapigment contribution to static disorder in transition energies can be neglected. In case of open-ring chromophores such as bilins, such a simple decription, most likely, would not be appropriate. Instead, one would have to take into account an intrinsic site energy shift that could only be calculated quantum chemically, and a new set of partial charges would have to be calculated for every conformation of the chromophore in order to describe the electrostatic interaction with the environment.

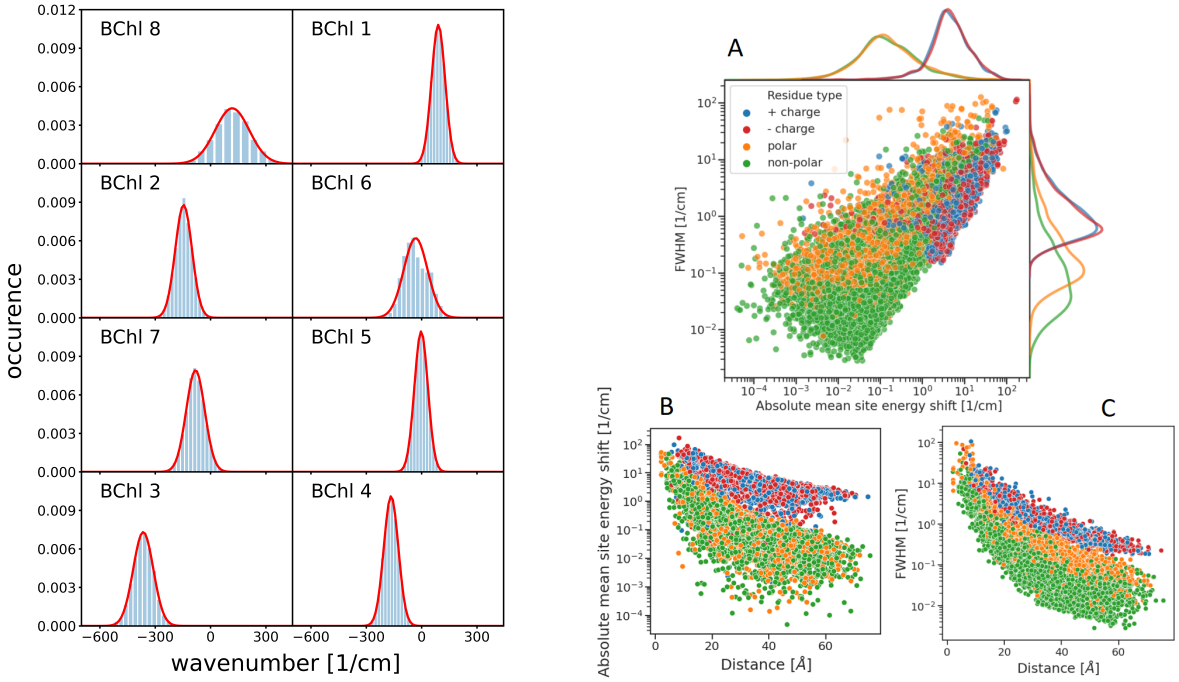

Figure 2: **Left:** Distribution of site energy shifts $\Delta E_m(c) = \sum_k \Delta E_m^{(k)}(c)$ (Eqs. 3 and 4) of the eight pigments BChl m ($m = 1, ..., 8$) in one monomeric subunit of the FMO protein, obtained by combining the FRODA Monte Carlo sampling of protein conformations and the CDC method for the calculation of site energy shifts. The red lines are Gaussian functions fitted to the histograms using the parameters in Table S1. **Right:** Analysis of site energy shifts $\Delta E_m^{(k)}(c)$ (Eq. 4) caused by single amino acid residues k of different type (blue, positively charged; red, negatively charged; orange, polar; green, non-polar). Panel A contains the correlation between the full width at half maximum (FWHM) of the distribution function of $\Delta E_m^{(k)}(c)$ and the absolute mean site energy shift $| < \Delta E_m^{(k)}(c) > |$. The curves on top and on the right side give the respective distribution functions for the various types of amino acids. Panels B and C contain the dependence of the FWHM and the $| < \Delta E_m^{(k)}(c) > |$, respectively, on the distance between amino acid k and pigment m.

The distribution of site energy shifts of the 8 BChl pigments of one monomeric subunit of

the FMO protein, obtained by applying the CDC method to 5200 different conformations of the PPC, computed with FRODA,[45] are shown in the left half of Fig. 2. These distribution functions can be well described by Gaussian functions of different widths (red lines), varying between 86 cm^{-1} for BChl 5 and 220 cm^{-1} for BChl 8 (Table S1). The large width of the latter reflects the large conformational flexibility of BChl 8, which is bound at the surface of the FMO protein, whereas all other BChls are packed closely inside a protein bag of mostly beta sheet secondary structures (Fig. 1). The inhomogeneous widths are in the same range as those suggested from the fit of optical spectra[16,17,19,21,42] and on the basis of QM/MM simulations with interpolated potential energy surfaces of the pigments.[33] Note, however, that in these approaches the estimation was more indirect, since the effect of dynamic disorder had to be evaluated as well.

The Gaussian functional form of the distribution functions suggests that the FMO protein obeys the central limit theorem. The latter states that a sum (Eq. 3) of independent random variables $\Delta E_m^{(k)}$ (Eq. 4), which may have different individual distribution functions characterized by a mean value $\langle \Delta E_m^{(k)} \rangle$ and variance $\sigma_{m,k}^2$, will be distributed by a Gaussian function of variance $s_m^2 = \sum_k \sigma_{m,k}^2$ centered at $\langle \Delta E_m \rangle = \sum_k \langle \Delta E_m^{(k)} \rangle$. This result holds only if none of the random variables $\Delta E_m^{(k)}$ in the sum over k (Eq. 3) is too dominant. A quantitative measure of this condition was provided, e.g., by Ljapunov and Lindeberg.[51,52]

In the case of the FMO protein, there are a lot of individual contributions $\Delta E_m^{(k)}$ from different amino acid residues k to the mean value $\langle \Delta E_m \rangle$ and the variance s_m of the site energy shift of pigments m (Fig. 2, right half). Interactions of the pigments with charged amino acid residues give large individual contributions (panel A) and exhibit the weakest distance dependence (panels B and C) as expected. Interestingly, the polar and the non-polar amino acid residues give very similar site energy shifts on average (top orange and green curves in panel A), whereas the contribution of the former to the width of the distribution function is significantly larger than that of the latter (right orange and green curves in panel A). This behavior is explained by the fact that polar side chains often exhibit different

rotamers, which give rise to opposite site energy shifts that cancel on average, but widen the distribution function.

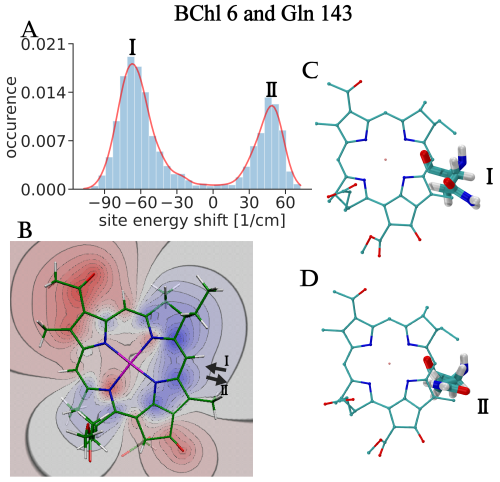

Figure 3: Site energy shift of BChl 6 caused by protein residue Gln 143. In panel A, the distribution function of this site energy shift is shown. The red line on top of the histograms was added to guide the eye. A structural explanation of the two peaks I and II of the distribution function is given in panels C-D. Panel B contains the difference electrostatic potential between the excited and the ground state of BChl *a* obtained with TD-DFT calculations using the B3LYP XC functional. Red (blue) regions correspond to negative (positive) difference potential. The two black arrows I and II represent the dipole moment of the amide side chain of Gln 143 in the two conformations I and II of this residue, which are shown in panels C and D.

An example is given in Fig. 3, where the contribution of Gln 143 to the site energy shift of BChl 6 is analyzed. Due to the two rotamers I and II (Fig. 3, panels C and D respectively), in which the polar amide group is oriented in opposite directions, a bimodal distribution function of the site energy shift results (Fig. 3A) with maxima I and II at roughly -70 and +50 cm^{-1}. In conformation I the negative end of the amide dipole of Gln 143 points toward the region of positive (excited minus ground state) difference potential of BChl 6, whereas in conformation II it is the positive end (Fig. 3B), causing a red and a blue-shift of the site energy, respectively.

For charged amino acids such a switch in the sign of the site energy shift for different rotamers is not observed, since the displacement of the charge is too small to enter regions of different sign of the difference potential of the pigments. A typical example is shown in

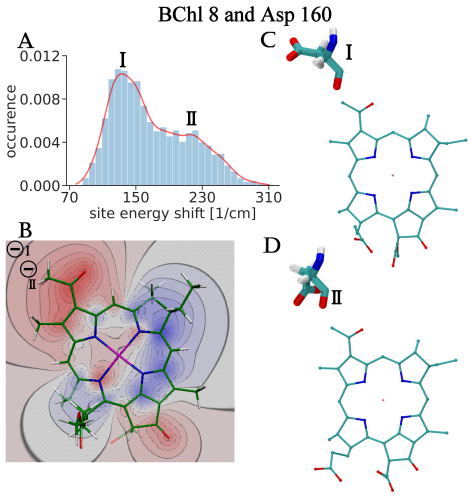

Figure 4: Same as in Fig. 3 but for BChl 8 and the negatively charged Asp 160. The two negative signs in the upper left corner of panel A illustrate the relative positions of the negative charge of Asp 160 in the two conformations.

Fig. 4. The distribution function of the site energy shift of BChl 8 caused by the negatively charged Asp 160 has a maximum at 140 cm^{-1} and a shoulder at 220 cm^{-1} (Fig. 4A). In the underlying conformations I and II, respectively, the negative charge is located in the negative region of the difference potential of BChl 8 (Fig. 4B), explaining the blue shift of the site energy. The larger blue shift in conformation II is explained by the smaller distance between the charge and the pigment.

It can be expected that the present calculations will help to pave the way for a microscopic understanding of single molecule and hole-burning spectra of PPCs, where the conformational transitions are detected as jumps of optical lines and antiholes, respectively.[53–57] The bimodal distribution function in Fig. 3 provides a first microscopic representation of the empirical bistable conformational substates usually assumed in the interpretation of these experiments.[53–55] In hole-burning experiments, the excess energy deposited in the pigment-protein complex by repeated near monochromatic optical excitation (burning) of a pigment drives conformational transitions of the local protein environment. According to the present calculations, a candidate for this conformational transition is the rotation of polar side groups of amino acid residues in the close neighborhood of the pigment, which lead to a change of

its transition energy (Fig. 3). The hole-burning signal is defined as the difference between the post- and the pre-burn absorption spectrum. Hence a negative (hole) / positive (antihole) difference signal is detected at the pre/post-burn transition energy of the pigment. Note, that the interpretation of such experiments is often complicated by the delocalization of excited states, which can, however, be taken into account.[56,57]

The maxima of the site energy shift distribution functions in Fig. 2 (left half) representing the mean site energy shifts of the pigments reveal the site energy funnel discovered earlier.[17,19–21] The pigments that are closer to the reaction center (BChls 3 and 4) are redshifted with respect to those that are located at the interface to the baseplate (BChls 8 and 1), which connects the FMO protein with the outer chlorosome antenna (Fig. 1). Indeed, there is an excellent correlation between the mean site energies, obtained here with FRODA/CDC and the reference values from the literature (upper part of Fig. S2), that were obtained from CDC calculations and a refinement fit of optical spectra.[21] A notable exception is the mean site energy of BChl 1, which is about 200 cm^{-1} larger than the reference value. A much weaker correlation is obtained between the present FRODA/CDC average site energies and ab-initio values from the literature[22,24,26] (lower part of Fig. S2), illustrating the challenges that a full ab-initio calculation is facing. The most encouraging results are obtained with a QM/MM method that uses a Shepard interpolation correction for the potential energy surfaces of the pigments.[24]

For the calculation of optical spectra, a lineshape theory that is based on time-local density matrix theory is used. In this theory, the diagonal elements of the exciton-vibrational coupling in the exciton basis are treated non-perturbatively and a Markov and secular approximation is used for the off-diagonal elements. The details of this theory are given in earlier work[58] and in the SI. Because BChl 8 is bound at the surface of the FMO protein, it is easily lost in the preparation of the complex. We have assumed an occupation of 35 % of the 8th site in the calculation of the spectra, as has been estimated from the crystal structure.[13] Note, however, that this number is highly uncertain, since it depends on the

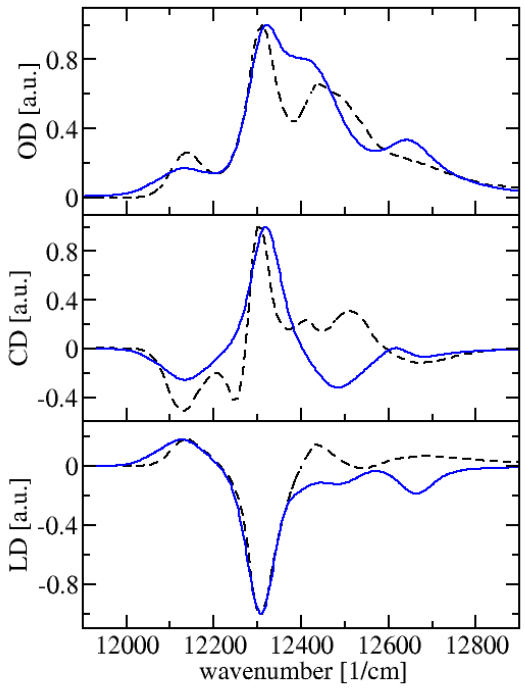

Figure 5: Calculations (blue solid lines) of low temperature (4 K) absorbance (top part), circular dichroism (middle part) and linear dichroism (lower part) spectra are compared with experimental data[42] (black dashed lines).

details of the sample preparation. So far, no systematic study is available on this subject. Fortunately, BChl 8 only affects the blue side of the spectrum in *P. aestuarii*.[21] Excitonic couplings are obtained first in point-dipole approximation for the crystal structure using an effective dipole strength of 30 D^2.[17]

The resulting low-temperature (4 K) linear absorption, circular dichroism and linear dichroism spectra of a monomeric subunit of the FMO protein are compared in Fig. 5 with experimental data,[42] revealing good agreement. Qualitative disagreement is only obtained at the blue wing of the spectrum and can be traced back to the site energy of BChl 1. A difference between BChl 1 and the remaining pigments is that the crystal structure suggests the formation of a hydrogen bond between the 3-acetyl group of this pigment and a nearby water molecule, which is broken in the FRODA conformations (Fig. S3). Earlier electrostatic

calculations suggest that this hydrogen bond red-shifts the site energy of BChl 1 by 120 cm^{-1} (SI, Table 4 of ref.[19]), which would improve the agreement between the calculated and experimental spectra in Fig. 5. Because of the uncertainty in the treatment of hydrogen bond networks involving water molecules, we have omitted all water molecules in the calculation of the site energy shifts. Including them leads to slightly less agreement with experimental spectra (Fig. S4), but has no qualitative influence.

In two other cases, BChls 2 and 3, there are some deviations in the site energies between the monomeric subunits of the FMO protein (Fig. S2), which can be traced back to hydrogen bonds of the 3-acetyl groups of BChls 2 and 3 with Ser 72 and Tyr 15, respectively. Whereas these hydrogen bonds are permanently formed in one monomer, they have a high probability of being broken in the other two monomers (Figs. S5 and S7). The resulting distribution functions of the site energy shift caused by the respective amino acid residue clearly demonstrate that there is a distinct red-shift of the site energy by the hydrogen bond (Figs. S6 and S8). It seems that the standard cutoff-value for fixing hydrogen bonds in FRODA is in between those found in the three monomeric subunits for these two BChls, after the originally C3 symmetric crystal structure has been geometry-optimized. The spectra of the monomer with the fixed hydrogen bond agree better with the experimental data than those calculated for the other two monomers (Fig. S9). In the case of Tyr 15, there is independent evidence for the presence of the hydrogen bond in the inhomogeneous ensemble from the mutagenesis studies[27] discussed above. The above examples show the limitations of the present FIRST/FRODA approach. A refinement of the Monte Carlo moves by using a potential energy function that includes electrostatic interactions could help to treat these hydrogen bonds in a more realistic way.

In a next step, we have investigated static disorder in the interpigment excitonic couplings. It is well known, that the point-dipole approximation (PDA) holds for the pigment positions in the crystal structure.[17,59] In order to take into account possible deviations from the PDA in our inhomogeneous ensemble, we have applied the transition charge from elec-

trostatic potential (TrEsp) method,[20] as described in the SI. Gaussian distribution functions are obtained for the couplings with mean values that, for most couplings, agree well with those obtained in PDA for the crystal structure (Table S4). The FWHM of the resulting ditribution functions of the large couplings are ~~in the 30 % range~~ of the average coupling values. For some pigment pairs with small interpigment distances and small excitonic couplings (e.g. 3-7 and 5-7), the FWHM of the distribution function is larger by a factor of up to 3 than the average coupling. Obviously, in these cases the mutual orientation of transition dipoles is unfavorable for strong coupling, but the coupling is more sensitive to conformational changes. The present results are very similar to those obtained earlier using the PDA in combination with FIRST and FRODA[44] (Table S4, Monomer 1), demonstrating the the PDA is valid for conformational substates of the present system. In agreement with the earlier work,[44] we find that the variations in excitonic couplings are so small that their effect on the inhomogeneous broadening of optical spectra is negligible (Fig. S9).

Finally, we have investigated the correlation in site energy variations between different BChls. The Pearson correlation coefficient is close to zero for all pigment pairs in all three monomeric subunits of the FMO protein (Fig. S10). Restricting the protein part in the site energy calculations to specific structural elements, correlations and anticorrelations appear. For example, the conformational changes of the backbone of one α-helix are found to cause an anticorrelated variation of the site energies of BChls 3 and 4 (Fig. S11). However, due to the large number of contributions to the site energy disorder, this correlation is washed out, if the whole protein is taken into account. In our earlier work, it has been hypothesized that correlated static disorder may lead to more efficient energy transfer, since the energy gaps between exciton states are kept small enough such that efficient energy dissipation can occur,[44,45] and that this correlation could be responsible for long-lived inter-exciton coherences found in 2D electronic spectroscopy.[39] The present finding (Fig. S10) excludes these hypotheses. It is the contribution of intramolecular and intermolecular vibrations to the spectral density, used for the description of dynamic disorder, that allows the protein

to dissipate smaller and larger portions of an exciton's excess energy throughout the full inhomogeneous width of the Q_y absorption spectrum.[17,39] The large number of degrees of freedom makes the PPC flexible enough for broad band dissipation without the need to restrict the energy gaps between exciton states.

The earlier study[45] was restricted by the number of conformations and the protein volume that could be included in the QC calculation, and the focus was put on the very low-frequency conformational motion extracted from the first principal component of the MC trajectories. In the present study, all these restrictions are lifted and the many contributions to the site energy correlations essentially average out. The fact that the line widths of the different exciton transitions agree qualitatively with the experimental line widths (Fig. 5) suggests that static disorder is well represented by the present FRODA trajectories without restricting these trajectories to certain principal components. In addition, this result shows that the intrapigment contributions to the site energy shifts, which are not taken into account in CDC calculations, most likely are more relevant for dynamic disorder (fast time scales) as expected.

Concerning the long-lived coherences found in 2D spectroscopy,[4–8] there is accumulating evidence that the origin is of vibrational rather than excitonic nature.[6–8,60,61] The most direct evidence was obtained in low-temperature 2D experiments on mutants by the Scholes and Blankenship groups.[6] In one of their experiments, they genetically exchanged the tyrosine, which forms a hydrogen bond to the 3-acetyl group of BChl 3. As discussed above, this mutation shifts the site energy of BChl 3 to the blue to an extent that the low-energy absorption band (dominated by BChl 3) disappears.[19,27] Nevertheless, no change in the frequency of coherent oscillations, that originally had been assigned to inter-exciton coherences between the lowest two exciton states,[4,5] was observed.[6] Recently, the Blankenship and Harel groups[8] detected a 60 fs decay of an inter-exciton coherence at physiological temperatures, which they identified as the one between exciton states 2 and 7. This decay time is in full agreement with recent theoretical estimates that assume uncorrelated static disorder in site

energies.[10] The justification for this assumption is provided here.

Acknowledgement

Support by the Austrian Science Fund (FWF) through grant P 33155 (T.R.) is gratefully acknowledged.

Supporting Information available

Hamiltonian of exciton-vibrational coupling, lineshape function of optical spectra, calculation of static disorder in excitonic couplings, structure of FMO trimer, correlation between mean site energies and reference values from the literature, analysis of hydrogen bond between BChl 1 and a water molecule, effect of water molecules on the optical spectra of the three monomeric subunits of the FMO protein, analysis of hydrogen bond between BChl 2 and Ser 72 and the resulting site energy shift, analysis of hydrogen bond between BChl 3 and Tyr 15 and the resulting site energy shift, effect of static disorder in excitonic couplings on the optical spectra, analysis of correlations in site energy fluctuations, including the effects caused by the backbone of two α helices, parameters of the Gaussian distribution functions in Fig. 2, atomic partial charges of the gound and excited state of BChl *a*, atomic transition charges of BChl *a*, excitonic couplings including characterization of static disorder.

References

(1) Brixner, T.; Stenger, J.; Vaswani, H. M.; Cho, M.; Blankenship, R. E.; Fleming, G. R. Two-dimensional spectroscopy of electronic couplings in photosynthesis. *Nature* **2005**, *434*, 625–628.

(2) Thyrhaug, E.; Zidek, K.; Dostal, J.; Bina, D.; Zigmantas, D. Exciton Structure and Energy Transfer in the Fenna-Matthews-Olson Complex . *J. Phys. Chem. Lett.* **2016**, *7*, 1653–1660.

(3) Dostal, J.; Psencik, J.; Zigmantas, D. *In situ* mapping of the energy flow through the entire photosynthetic apparatus. *Nature Chem.* **2016**, *8*, 705–710.

(4) Engel, G. S.; Calhoun, T. R.; Read, E. L.; Ahn, T.-K.; Mancal, T.; Cheng, Y.-C.; Blankenship, R. E.; Fleming, G. R. Evidence for wavelike energy transfer through quantum coherence in photosynthetic systems. *Nature* **2007**, *446*, 782–786.

(5) Panitchayangkoon, G.; Hayes, D.; Fransted, K. A.; Caram, J. R.; Wen, J.; Blankenship, R. E.; Engel, G. S. Long-lived quantum coherence in photosynthetic complexes at physiological temperature. *Proc. Natl. Acad. Sci. USA* **2010**, *107*, 12766–12770.

(6) Maiuri, M.; Ostroumov, E. E.; Saer, R. G.; Blankenship, R. E.; Scholes, G. D. Coherent wavepackets in the Fenna-Matthews-Olson complex are robust to excitonic-structure perturbations caused by mutagenesis. *Nature Chem.* **2018**, *10*, 177–183.

(7) Thyrhaug, E.; Tempelaar, R.; Alcocer, M. J.; Zidek, K.; Bina, D.; Knoester, J.; Jansen, T. L. C.; Zigmantas, D. Identification and characterization of diverse coherences in the Fenna-Matthews-Olson complex . *Nature Chem.* **2018**, *10*, 780–786.

(8) Irgen-Gioro, S.; Gururangan, K.; Saer, R. G.; Blankenship, R. E.; Harel, E. Electronic coherence lifetimes of the Fenna-Matthews-Olson complex and light harvesting complex II. *Chem. Sci.* **2019**, *10*, 10503–10509.

(9) Fleming, G. R.; Scholes, G. D.; Cheng, Y. C. Quantum effects in biology. *Procedia Chemistry* **2011**, *3*, 38–57.

(10) Cao, J.; Cogdell, R. J.; Coker, D. F.; Duan, H.-G.; Hauer, J.; Kleinekathöfer, U.; Jansen, T. L. C.; Mancal, T.; Miller, R. J. D.; Ogilvie, J. P. et al. Quantum Biology Revisited. *Science Advances* **2020**, *6*, eaaz4888.

(11) Renger, T.; Müh, F. Understanding photosynthetic light-harvesting: a bottom up theoretical approach. *Phys. Chem. Chem. Phys.* **2013**, *15*, 3348–3371.

(12) Mennucci, B.; Corni, S. Multiscale modelling of photoinduced processes in composite systems. *Nat. Rev. Chem.* **2019**, *3*, 315–330.

(13) Tronrud, D. E.; Wen, J.; Gay, L.; Blankenship, R. E. The structural basis for the difference in absorbance spectra for the FMO antenna protein from various green sulfur bacteria . *Photosynth. Res.* **2009**, *100*, 79–87.

(14) Humphrey, W.; Dalke, A.; Schulten, K. VMD-Visual Molecular Dynamics. *J. Mol. Graphics* **1996**, *14*, 33–38.

(15) Milder, M. T. W.; Brüggemann, B.; van Grondelle, R.; Herek, J. L. Revisiting the optical properties of the FMO protein. *Photosynth. Res.* **2010**, *104*, 257274.

(16) Louwe, R. J. W.; Vrieze, J.; Hoff, A. J.; Aartsma, T. J. Toward an integral interpretation of the optical steady-state spectra of the FMO-complex of *Prosthecochloris aestuarii*. 2. Exciton simulations. *J. Phys. Chem. B* **1997**, *101*, 11280–11287.

(17) Adolphs, J.; Renger, T. How proteins trigger excitation energy transfer in the FMO complex of green sulfur bacteria. *Biophys. J.* **2006**, *91*, 2778–2797.

(18) Wen, J.; Zhang, H.; Gross, M. L.; Blankenship, R. E. Membrane orientation of the FMO antenna protein from *Chlorobaculum tepidum* as determined by mass spectrometry-based footprinting . *Proc. Natl. Acad. Sci. USA* **2009**, *106*, 6134–6139.

(19) Müh, F.; Madjet, M. E.; Adolphs, J.; Abdurahman, A.; Rabenstein, B.; Ishikita, H.; Knapp, E. W.; Renger, T. α-helices direct excitation energy flow in the Fenna-Matthews-Olson protein. *Proc. Natl. Acad. Sci. USA* **2007**, *104*, 16862–16867.

(20) Adolphs, J.; Müh, F.; Madjet, M. E.; Renger, T. Calculation of pigment transition energies in the FMO protein: From simplicity to complexity and back (erratum: https://doi.org/10.1007/s11120-007-9276-8) . *Photosynth. Res.* **2008**, *95*, 197–209.

(21) Schmidt am Busch, M.; Müh, F.; Madjet, M. E.; Renger, T. The Eighth Bacteriochlorophyll Completes the Excitation Energy Funnel in the FMO Protein. *J. Phys. Chem. Lett.* **2011**, *2*, 93–98.

(22) Jurinovich, S.; Curutchet, C.; Mennucci, B. The Fenna-Matthews-Olson Protein Revisited: A Fully Polarizable (TD)DFT/MM Description. *Chem. Phys. Chem.* **2014**, *15*, 3194–3204.

(23) Goez, A.; Jacob, C. R.; Neugebauer, J. Modeling environment effects on pigment site energies: Frozen density embedding with fully quantum-chemical protein densities. *Comp. Theor. Chem.* **2014**, *1040*.

(24) Saito, S.; Higashi, M.; Fleming, G. R. Site-Dependent Fluctuations Optimize Electronic Energy Transfer in the Fenna-Matthews-Olson Protein. *J. Phys. Chem. B* **2019**, *123*, 9762–9772.

(25) Kaliakin, D. S.; Nakata, H.; Kim, Y.; Chen, Q.; Fedorov, D. G.; Slipchenko, L. V. FMOxFMO: Elucidating Excitonic Interactions in the Fenna-Matthews-Olson Complex with the Fragment Molecular Orbital Method. *J. Chem. Theo. Comp.* **2020**, *16*, 1175–1187.

(26) Kim, Y.; Morozov, D.; Stadnytski, S., V. Savikhin; Slipchenko, L. V. Predictive First-Principles Modeling of a Photosynthetic Antenna Protein: The Fenna-Matthews-Olson Complex. *J. Phys. Chem. Lett.* **2020**, *11*, 1636–1643.

(27) Saer, R. G.; Stadnytskyi, V.; Magdaong, N. C.; Goodson, C.; Savikhin, S.; Blankenship, R. E. Probing the excitonic landscape of the *Chlorobaculum tepidum* Fenna-Matthews-Olson (FMO) complex: a mutagenesis approach. *Biochim. Biophys. Acta* **2017**, *1858*, 288–296.

(28) Olbrich, C.; Strümpfer, J.; Schulten, K.; Kleinekathöfer, U. Theory and simulation of

the environmental effects on FMO electronic transitions. *J. Phys. Chem. Lett.* **2011**, *2*, 1771–1776.

(29) Rivera, E.; Montemayor, D.; Masia, M.; Coker, D. F. Influence of site-dependent pigmentprotein interactions on excitation energy transfer in photosynthetic light harvesting. *J. Phys. Chem. B* **2013**, *117*, 5510–5521.

(30) Chandrasekran, S.; Aghtar, M.; Valleau, S.; Aspuru-Guzik, A.; Kleinekathöfer, U. Influence of Force Fields and Quantum Chemistry Approach on Spectral Densities of BChl *a* in Solution and in FMO Proteins. *J. Phys. Chem. B* **2015**, *119*, 9995–10004.

(31) Lee, M. K.; Coker, D. F. Modeling Electronic-Nuclear Interactions for Excitation Energy Transfer Processes in Light-Harvesting Complexes. *J. Phys. Chem. Lett.* **2016**, *7*, 3171–3178.

(32) Kim, C. W.; Rhee, Y. M. Constructing an Interpolated Potential Energy Surface of a Large Molecule: A Case Study with Bacteriochlorophyll *a* Model in the Fenna-Matthews-Olson Complex. *J. Chem. Theory Comput.* **2016**, *12*, 5235–5246.

(33) Kim, C. W.; Choi, B.; Rhee, Y. M. Excited state energy fluctuations in the Fenna-Matthews-Olson complex from molecular dynamics simulations with interpolated chromophore potentials. *Phys. Chem. Chem. Phys.* **2018**, *20*, 3310–3319.

(34) Jing, Y.; Zheng, R.; Li, H.-X.; Shi, Q. Theoretical Study of the Electronic-Vibrational Coupling in the Q_y States of the Photosynthetic Reaction Center in Purple Bacteria. *J. Phys. Chem. B* **2011**, *116*, 1164–1171.

(35) Rosnik, A. M.; Curutchet, C. Theoretical Characterization of the Spectral Density of the Water- Soluble Chlorophyll-Binding Protein from Combined Quantum Mechanics/Molecular Mechanics Molecular Dynamics Simulations. *J. Chem. Theory Comput.* **2015**, *11*, 5826–5837.

(36) Higashi, M.; Saito, S. Quantitative Evaluation of Site Energies and Their Fluctuations of Pigments in the Fenna-Matthews-Olson Complex with an Efficient Method for Generating a Potential Energy Surface. *J. Chem. Theory Comput.* **2016**, *12*, 4128–4137.

(37) Blau, S. M.; Benneth, D. I. G.; Kreisbeck, C.; Aspuru-Guzik, A. Local protein solvation drives direct down-conversion in phycobiliprotein PC645 via incoherent vibronic transport. *Proc. Natl. Acad. Sci. USA* **2018**, *115*, E3342–E3350.

(38) Maity, S.; Bold, B. M.; Prajapati, J. D.; Sokolov, M.; Kubar, T.; Elstner, M.; Kleinekathöfer, U. DFTB/MM Molecular Dynamics Simulations of the FMO Light-Harvesting Complex. *Phys. Chem. Lett.* **2020**, *11*, 8660–8667.

(39) Renger, T.; Klinger, A.; Steinecker, F.; Schmidt am Busch, M.; Numata, J.; Müh, F. Normal Mode Analysis of the Spectral Density of the Fenna-Matthews-Olson Light-Harvesting Protein: How the Protein Dissipates the Excess Energy of Excitons. *J. Phys. Chem. B* **2012**, *116*, 14565–14580.

(40) Cupellini, L.; Caprasecca, S.; Guido, C. A.; Müh, F.; Renger, T. Coupling to Charge Transfer States is the Key to Modulate the Optical Bands for Efficient Light Harvesting in Purple Bacteria. *J. Phys. Chem. Lett* **2018**, *9*, 6892–6899.

(41) Slama, V.; Cupellini, L.; Mennucci, B. Exciton properties and optical spectra of light harvesting complex II from a fully atomistic description. *Phys. Chem. Chem. Phys.* **2020**, *22*, 16783–16795.

(42) Wendling, M.; Przyjalgowski, M. A.; Gülen, D.; Vulto, S. I. E.; Aartsma, T. J.; van Grondelle, R.; van Amerongen, H. The quantitative relationship between structure and polarized spectroscopy in the FMO complex of *Prosthecochloris aestuarii*: refining experiments and simulations. *Photosynth. Res.* **2002**, *71*, 99–123.

(43) Wells, S.; Menor, S.; Hespenheide, B.; Thorpe, M. F. Constrained geometric simulation of diffusive motion in proteins. *Phys. Biol.* **2005**, *2*, S127–S136.

(44) Fokas, A. S.; Cole, D. J.; Chin, A. W. Constrained geometric dynamics of the Fenna-Matthews-Olson complex: the role of correlated motion in reducing uncertainty in excitation energy transfer. *Photosynth. Res.* **2014**, *122*, 275–292.

(45) Fokas, A. S.; Cole, D. J.; Hine, N. D. M.; Wells, S. A.; Payne, M. C.; Chin, A. W. Evidence of Correlated Static Disorder in the Fenna-Matthews-Olson Complex. *J. Phys. Chem. Lett.* **2017**, *8*, 2350–2356.

(46) Madjet, M. E.; Abdurahman, A.; Renger, T. Intermolecular Coulomb couplings from ab initio electrostatic potentials: application to optical transitions of strongly coupled pigments in photosynthetic antennae and reaction centers. *J. Phys. Chem. B* **2006**, *110*, 17268–17281.

(47) Olbrich, C.; Strümpfer, J.; Schulten, K.; Kleinekathöfer, U. Quest for Spatially Correlated Fluctuations in the FMO Light-Harvesting Complex. *J. Phys. Chem. B* **2011**, *115*, 758–764.

(48) Jacobs, D. J.; Rader, A. J.; Kuhn, L. A.; Thorpe, M. F. Protein Felexibility Predictions Using Graph Theory. *Proteins* **2001**, *44*, 150–165.

(49) MacKerell Jr., A. D.; Bashford, D.; Bellott, M.; Dunbrack Jr., R. L.; Evanseck, J. D.; Field, M. J.; Fischer, S.; Gao, J.; Guo, H.; Ha, S. et al. All-atom empirical potential for molecular modeling and dynamics studies of proteins. *J. Phys. Chem. B* **1998**, *102*, 3586–3616.

(50) Eaton, J. W.; Bateman, D.; Hauberg, S.; Wehbring, R. GNU Octave version 5.1.0 manual: a high-level interactive language for numerical computations. 2019.

(51) Lindeberg, J. W. Eine neue Herleitung des Exponentialgesetzes in der Wahrscheinlichkeitsrechnung (in German). *Mathematische Zeitschrift* **1922**, *15*, 211–225.

(52) Le Cam, L. The Central Limit Theorem around 1935. *Statistical Science* **1986**, *1*, 78–91.

(53) Jankowiak, R.; Hayes, J. M.; Small, G. J. Spectral Hole-Burning Spectroscopy in Amorphous Molecular Solids and Proteins. *Chem. Rev.* **1993**, *93*, 1471–1502.

(54) Purchase, R.; Völker, S. Spectral hole burning: examples from photosynthesis. *Photosynth. Res.* **2009**, *101*, 245–266.

(55) Jankowiak, R.; Reppert, M.; Zazubovich, V.; Pieper, J.; Reinot, T. Site Selective and Single Complex Laser-Based Spectroscopies: A Window on Excited State Electronic Structure, Excitation Energy Transfer and Electron-Phonon Coupling of Selected Photosynthetic Complexes. *Chem. Rev.* **2011**, *111*, 4546–4598.

(56) Reppert, M. Modeling of Resonant Hole-Burning Spectra in Excitonically Coupled Systems: The Effects of Energy-Transfer Broadening. *J. Phys. Chem. Lett.* **2011**, *2*, 2716–2721.

(57) Adolphs, J.; Berrer, M.; Renger, T. Hole-Burning Spectroscopy on Excitonically Coupled Pigments in Proteins: Theory Meets Experiment. *J. Am. Chem. Soc.* **2016**, *138*, 2993–3001.

(58) Renger, T.; Marcus, R. A. On the relation of protein dynamics and exciton relaxation in pigment-protein complexes: an estimation of the spectral density and a theory for the calculation of optical spectra. *J. Chem. Phys.* **2002**, *116*, 9997–10019.

(59) Renger, T. Theory of excitation energy transfer: from structure to function. *Photosynth. Res.* **2009**, *102*, 471–485.

(60) Tiwari, V.; Peters, W. K.; Jonas, D. M. Electronic resonance with anticorrelated pigment vibrations drives photosynthetic energy transfer outside the adiabatic framework. *Proc. Natl. Acad. Sci. U.S.A.* **2013**, *110*, 1203–1208.

(61) Duan, H.-G.; Prokhorenko, V. I.; Cogdell, R. J.; Ashraf, K.; Stevens, A. L.; Throwart, M.; Miller, R. J. D. Nature does not rely on long-lived electronic quan-

tum coherence for photosynthetic energy transfer. *Proc. Natl. Acad. Sci. USA* **2017**, *114*, 8493–8498.